Disruption of vascular Ca^{2+}-activated chloride currents lowers blood pressure

Christoph Heinze,[1] Anika Seniuk,[2] Maxim V. Sokolov,[3] Antje K. Huebner,[1] Agnieszka E. Klementowicz,[3] István A. Szijártó,[4,5] Johanna Schleifenbaum,[4] Helga Vitzthum,[2] Maik Gollasch,[4] Heimo Ehmke,[2] Björn C. Schroeder,[3] and Christian A. Hübner[1]

[1]Institut für Humangenetik, Universitätsklinikum Jena, Friedrich-Schiller Universität Jena, Jena, Germany. [2]Institut für Zelluläre und Integrative Physiologie, Universitätsklinikum Hamburg Eppendorf, Hamburg, Germany. [3]Max-Delbrück Centrum für Molekulare Medizin (MDC) and NeuroCure, Berlin, Germany. [4]Medizinische Klinik mit Schwerpunkt Nephrologie und Internistische Intensivmedizin, Charité – Universitätsmedizin Berlin, Experimental and Clinical Research Center (ECRC), Berlin, Germany. [5]Interdisziplinäres Stoffwechsel-Centrum, Charité – Universitätsmedizin Berlin, Berlin, Germany.

High blood pressure is the leading risk factor for death worldwide. One of the hallmarks is a rise of peripheral vascular resistance, which largely depends on arteriole tone. Ca^{2+}-activated chloride currents (CaCCs) in vascular smooth muscle cells (VSMCs) are candidates for increasing vascular contractility. We analyzed the vascular tree and identified substantial CaCCs in VSMCs of the aorta and carotid arteries. CaCCs were small or absent in VSMCs of medium-sized vessels such as mesenteric arteries and larger retinal arterioles. In small vessels of the retina, brain, and skeletal muscle, where contractile intermediate cells or pericytes gradually replace VSMCs, CaCCs were particularly large. Targeted disruption of the calcium-activated chloride channel TMEM16A, also known as ANO1, in VSMCs, intermediate cells, and pericytes eliminated CaCCs in all vessels studied. Mice lacking vascular TMEM16A had lower systemic blood pressure and a decreased hypertensive response following vasoconstrictor treatment. There was no difference in contractility of medium-sized mesenteric arteries; however, responsiveness of the aorta and small retinal arterioles to the vasoconstriction-inducing drug U46619 was reduced. TMEM16A also was required for peripheral blood vessel contractility, as the response to U46619 was attenuated in isolated perfused hind limbs from mutant mice. Out data suggest that TMEM16A plays a general role in arteriolar and capillary blood flow and is a promising target for the treatment of hypertension.

Introduction

With more than 25% of the adult population being affected, hypertension is an important public health challenge worldwide (1). It is a major risk factor for cardiovascular disease, myocardial infarction, stroke, and chronic renal failure. The pathogenesis of hypertension as well as the basic mechanisms of blood pressure control, however, are still insufficiently understood. A hallmark of hypertension is the increased tone of arterial blood vessels and therefore elevation of total peripheral vascular resistance (2).

Vascular tone depends on a complex interplay of vasodilator and vasoconstrictor stimuli, which are integrated by VSMCs and transformed into the activity of the contractile apparatus. Accumulation of Cl^- by the Na^+-K^+-$2Cl^-$ co-transporter NKCC1 (3) and the Cl^-/HCO_3 exchanger AE2 (4) raises the Cl^- equilibrium potential above the resting membrane potential in VSMCs. Therefore, opening of Cl^- channels within the plasma membrane of VSMCs is predicted to cause Cl^- efflux and membrane depolarization (5). Ca^{2+}-activated chloride currents (CaCCs) have been described in VSMCs of various blood vessels (4, 6, 7). Because CaCC-dependent depolarization can activate voltage-gated Ca^{2+} channels and thus further increase intracellular Ca^{2+}, CaCCs may enhance the contractile response of blood vessels (8).

Recently, it has been shown that TMEM16A, also known as ANO1, mediates CaCCs (9–11). TMEM16A belongs to a family of 10 homologous transmembrane proteins of approximately 900 amino acids. So far four members have been shown to be associated with hereditary disorders, including craniocervical dystonia (12), muscular dystrophy (13), the bleeding disorder Scott syndrome (14), and cerebellar ataxia (15). Despite their obvious physiological importance, a function in ion transport has not been established for most family members. Interestingly, TMEM16F and other family members have been associated with scramblase activity (16). TMEM16A expression has been reported for VSMCs of the thoracic aorta, the carotid artery, and some arteries in the brain, and it has been suggested that TMEM16A mediates CaCCs of these cells (17, 18). Knockdown of TMEM16A in cultured medium-sized cerebral arteries from rat resulted in a reduction of pressure-induced vasoconstriction (19). Moreover whole-cell patch-clamp studies showed that knockdown of TMEM16A attenuated CaCCs in rodent large cerebral artery VSMCs (20, 21). However, the role of CaCCs in VSMCs in the regulation of systemic arterial blood pressure could not be addressed so far, as *Tmem16a* knockout mice have a complex phenotype with early mortality, malformations of the trachea, and intestinal obstruction (22). Moreover, specific CaCC inhibitors are currently not available.

Here we show that disruption of TMEM16A under the control of the smooth myosin heavy chain promoter abolishes CaCCs in contractile cells of blood vessels and lowers arterial blood pressure. This hypotensive effect of disruption of TMEM16A is most likely mediated via small-diameter arterioles, where CaCCs are particularly large and contribute to vascular contractility and thus to peripheral resistance.

Authorship note: Christoph Heinze, Anika Seniuk, and Maxim V. Sokolov contributed equally to this work.

Conflict of interest: The authors have declared that no conflict of interest exists.

Citation for this article: *J Clin Invest.* 2014;124(2):675–686. doi:10.1172/JCI70025.

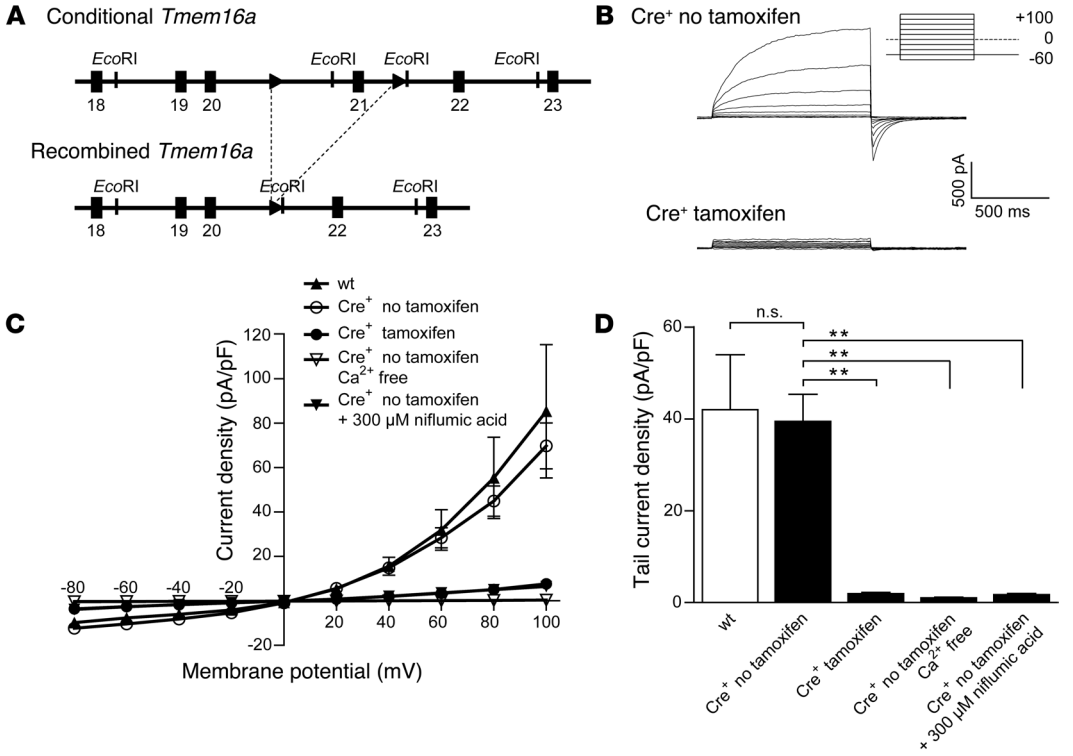

Figure 1

Disruption of TMEM16A under the control of the smooth muscle myosin heavy chain promoter abolishes CaCCs in VSMCs of the aorta. (**A**) In the targeted *Tmem16a* locus, exon 21 is flanked by loxP sites (upper panel). After Cre-mediated excision, the floxed fragment is removed (lower). Numbered black squares represent exons and triangles, loxP sites; *Eco*RI restriction sites used for cloning/screening are indicated. (**B**) Typical currents recorded from VSMCs isolated from thoracic aortae of non-induced control mice (Cre^+ no tamoxifen) and induced conditional *Tmem16a* knockout mice (Cre^+ tamoxifen). Inset: Voltage protocol. (**C**) CaCCs were absent in VSMCs isolated from the aorta of induced knockout mice. Mean I-V relationship was recorded after a 1 second test pulse from VSMCs isolated from thoracic aortae of WT, non-induced control (Cre^+ no tamoxifen), and induced conditional *Tmem16a* knockout mice (Cre^+ tamoxifen). CaCCs measured from controls were absent under Ca^{2+}-free conditions (Cre^+ no tamoxifen Ca^{2+} free). CaCCs of VSMCs were blocked by 300 μM niflumic acid (Cre^+ no tamoxifen + 300 μM niflumic acid). n = 6–15 cells each. (**D**) Amplitude of various VSMC tail current densities measured after a voltage step to –80 mV from a 1 second test pulse at +80 mV (n = 6–15 cells each). Whereas no difference was detected between non-induced control and wild-type mice, non-induced control mice and mice under other conditions differed significantly. 2-way ANOVA; $^{**}P < 0.01$.

Results

Disruption of TMEM16A eliminates CaCCs in VSMCs from the aorta. To overcome the limitations of the constitutive *Tmem16a* knockout mouse, we floxed exon 21 of the *Tmem16a* gene (Figure 1A), which encodes the most conserved part of the TMEM16 family (Supplemental Figure 1A; supplemental material available online with this article; doi:10.1172/JCI70025DS1). A cDNA construct devoid of exon 21 transfected into HEK cells did not give rise to CaCCs, whereas large CaCCs were observed upon transfection with the wild-type cDNA (Supplemental Figure 1, B–E), illustrating that the part of the protein encoded by exon 21 is essential for channel function. The floxed (*Tmem16a*$^{fl/fl}$) line was subsequently mated with either a Cre-deleter line (23) to generate constitutive TMEM16A mutant mice or the tamoxifen-inducible SMMHC-*Cre*-ER^{T2} line, which allows induction of Cre recombinase activity in the contractile cells of blood vessels by administration of tamoxifen (24). *Tmem16a* knockout mice with a homozygous deletion of exon 21 had malformations of the trachea (Supplemental Figure 1F) and died within the first 2 weeks of life, mirroring the phenotype previously reported for a constitutive *Tmem16a* knockout mouse model obtained by deletion of exon 12 (22). In VSMCs isolated from the aorta of non-induced conditional knockout mice, robust CaCCs were present, which depended on the presence of intracellular Ca^{2+} and could be blocked by niflumic acid, an inhibitor of CaCCs (Figure 1, B–D). CaCCs were absent in VSMCs isolated from mice after tamoxifen induction, indicating that this current is indeed mediated by TMEM16A (Figure 1, B–D).

Disruption of TMEM16A under the control of the SMMHC promoter has a hypotensive effect. We next addressed the role of vascular TMEM16A in vivo by measuring mean arterial blood pressure in a cohort of Cre-positive floxed mice fed on a diet supplemented with tamoxifen for 4 weeks (25) (Cre^+ tamoxifen). A control cohort of Cre-positive floxed mice did not receive tamoxifen (Cre^+ no tamoxifen). Mean arterial blood pressure (Figure 2A) and pressure amplitude (Figure 2B) decreased upon tamoxifen-induced disruption of TMEM16A when compared with non-induced controls, consistent with TMEM16A being an important regulator of vascular resistance. A control group that did not carry the SMMHC-Cre-ER^{T2} transgene (Cre^- tamoxifen) (Figure 2A) exhibited no change in mean arterial blood pressure upon tamoxifen treatment, ruling out a Cre-independent effect of tamoxifen on arterial blood pressure. An effect of activated Cre-ER^{T2} was

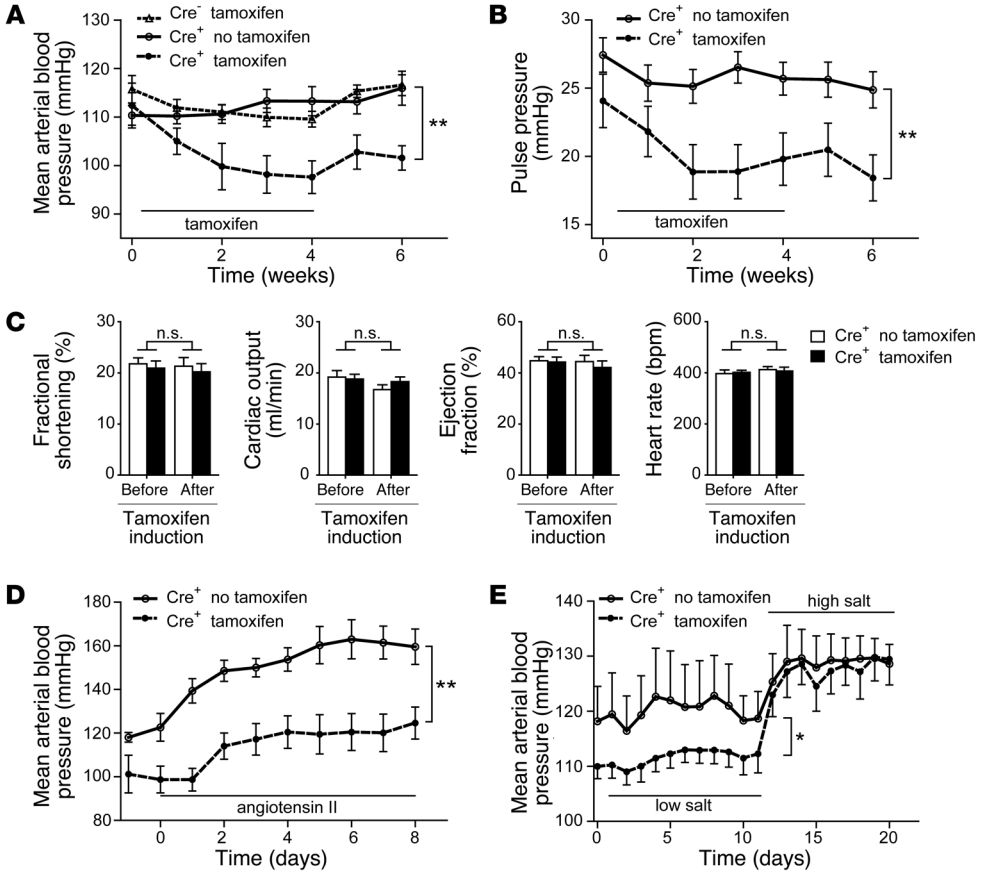

Figure 2

Disruption of TMEM16A in blood vessels decreases mean arterial blood pressure. (**A**) Blood pressure in three cohorts of floxed *Tmem16a* mice. Cre recombinase expressed under control of the SMMHC promoter was induced by feeding tamoxifen to the experimental cohort (Cre^+ tamoxifen, $n = 14$). Littermates of the same genotype that did not receive tamoxifen served as a control (Cre^+ no tamoxifen, $n = 15$). A Cre-negative control cohort received tamoxifen to exclude a gene-independent effect of tamoxifen on mean arterial blood pressure (Cre^- tamoxifen, $n = 6$). Induction with tamoxifen caused a significant decrease in systemic blood pressure in the Cre^+ cohort (2-way ANOVA; $^{**}P < 0.01$. (**B**) At the same time, the pulse pressure decreased (2-way ANOVA; $^{**}P < 0.01$). (**C**) Fractional shortening, cardiac output, ejection fraction, and heart rate did not differ between cohorts before and 2 weeks after termination of the tamoxifen induction. Student's *t* test. (**D**) The hypotensive effect of TMEM16A disruption on mean arterial blood pressure was enhanced in the presence of the vasopressor angiotensin II, which was continuously infused ($1.5\ ng*g^{-1}*min^{-1}$) with osmotic mini pumps starting 2 weeks after tamoxifen induction ($n = 6$–7 for each cohort). 2-way ANOVA; $^{**}P < 0.01$. (**E**) Mean arterial blood pressure did not further decrease on a low-salt diet. Switching to a high-salt diet eliminated the difference in blood pressure between induced and non-induced mice ($n = 4$ for each group). 2-way ANOVA; $^{*}P < 0.05$.

excluded by monitoring blood pressure during tamoxifen induction in mice carrying the SMMHC-Cre-ER^{T2} transgene on a wild-type background (data not shown). Cardiac parameters such as fractional shortening, cardiac output, ejection fraction, and heart rate were unchanged 2 weeks after termination of tamoxifen treatment and did not differ between controls and mutant mice (Figure 2C). Importantly, the hypotensive effect of the disruption of TMEM16A was maintained and even increased in the presence of the vasopressor angiotensin II (Figure 2D).

We subsequently addressed whether the hypotensive effect of TMEM16A disruption was dietary salt dependent. Although the hypotensive effect of TMEM16A disruption was not further increased by a low-salt diet, the difference in systemic blood pressure was eliminated on a high-salt diet (Figure 2E).

Plasma aldosterone, renin, angiotensin II, K^+, and various blood gas parameters analyzed did not differ between genotypes, excluding a major renal compensation via the renin-angiotensin-aldosterone system (Table 1). We also determined creatinine clearance and fractional excretion for Na^+, Cl^-, and K^+, but did not detect any significant differences between groups (Table 1).

TMEM16A and CaCCs are differentially expressed along the vascular tree. With a novel TMEM16A antibody directed against the N-terminal part of the protein, we assessed TMEM16A expression in different blood vessels by Western blot analysis. The WT TMEM16A signal, which runs at roughly 120 kDa, was shifted to a smaller size in the mutant (Figure 3, A and B). Notably, Western blot analysis as well as immunohistochemistry suggested that TMEM16A expression was lower in smaller compared with larger arteries (Figure 3, A, B, and D–F). In accordance with our expression analysis, CaCCs recorded from VSMCs isolated from the carotid and superior mesenteric artery were small compared with those from the aorta and even smaller in higher-order branches of the superior mesenteric artery (Figure 3C). CaCCs were absent in VSMCs isolated from our induced conditional knockout model (Figure 3C).

Table 1
Blood biochemistry and basic analysis of kidney function of non-induced control and induced conditional *Tmem16a* knockout mice

	No tamoxifen	*n*	Tamoxifen	*n*	*P*
Plasma hormone levels					
Renin (ng angiotensin I/ml/h)	25.25 ± 4.89	19	26.40 ± 4.57	21	NS
Angiotensin II (pg/ml)	4.27 ± 1.14	11	3.74 ± 1.49	9	NS
Aldosterone (pg/ml)	22.51 ± 9.06	18	15.61 ± 4.84	20	NS
ANP (ng/ml)	4.17 ± 0.23	14	4.20 ± 0.45	14	NS
Plasma electrolyte levels					
Na^+ (mmol/l)	149.15 ± 0.68	10	147.70 ± 1.22	10	NS
K^+ (mmol/l)	5.37 ± 0.19	10	5.21 ± 0.15	10	NS
Cl^- (mmol/l)	119.30 ± 0.68	10	119.30 ± 1.07	10	NS
Renal function					
Creatinine clearance (ml/24 h)	2,288.67 ± 1,139.78	9	2,023.66 ± 642.17	10	NS
Na^+ FE (%)	0.174 ± 0.055	9	0.206 ± 0.051	10	NS
K^+ FE (%)	5.48 ± 1.25	9	6.91 ± 1.47	10	NS
Cl^- FE (%)	0.0385 ± 0.0101	9	0.0545 ± 0.0146	10	NS

Data are shown as mean and SEM. FE, fractional excretion. Student's *t* test; $P > 0.05$.

Disruption of TMEM16A in VSMCs reduces contractility in aorta, but not in mesenteric arteries. We analyzed the wall-to-lumen ratio of blood vessels after disruption of TMEM16A, but did not observe any structural changes (Supplemental Figure 2, A and B). The response of aortic rings to various concentrations of external KCl did not differ between cohorts (Supplemental Figure 2, C and D). We measured the constriction of mesenteric arteries at 60 mM KCl, which was unchanged as well (Supplemental Figure 2, E and F). These results argue against a principal defect of voltage-gated Ca^{2+} channel–dependent vascular smooth muscle contraction upon disruption of TMEM16A. We next tested our hypothesis that vascular contractility is modulated by TMEM16A and compared the effects of various vasoconstrictors on aortic rings or rings isolated from first- and second-order mesenteric arteries of induced and non-induced mice. Changes in vessel tension of aortic rings from tamoxifen-induced mice in response to vasoconstrictor GPCR agonists such as angiotensin II (Figure 3G), U46619, a synthetic analog of prostaglandin PGH_2 (Figure 3J), and phenylephrine (Supplemental Figure 2G) were attenuated. In accordance with smaller or even absent CaCCs in first- and second-order mesenteric arteries, contraction of isolated first- and second-order mesenteric artery rings to vasopressors as assessed by wire myography did not differ between genotypes (Figure 3, H and K, and Supplemental Figure 2H). Similarly, constriction of third- and fourth-order mesenteric arteries as assessed by videomicroscopy did not differ between cohorts (Figure 3, I and L, and Supplemental Figure 2I). These data are supported by previous reports showing strong CaCCs in large vessels such as pulmonary artery, aorta, and portal vein but not in medium-sized vessels (4).

CaCCs in pericytes of small arterioles from brain and retina are mediated by TMEM16A and regulate their contractility. Because large conduit arteries only marginally contribute to peripheral resistance (26), the difference in arterial blood pressure upon disruption of TMEM16A cannot be explained by the decreased contractility of the aorta. Instead, the regulation of peripheral resistance largely depends on the diameter of smaller arterioles. During arborization of arterioles, VSMCs are gradually replaced by smooth muscle cell–like cells, which are termed intermediate cells or pericytes (27, 28). Pericytes had been reported to exhibit native currents (29) that are compatible with CaCCs. Indeed, microvessels in the brain, which are known to be densely packed with pericytes (30), showed marked immunoreactivity for TMEM16A (Figure 4A). Also, intermediate cells/pericytes of secondary and higher-order arterioles in the retina were intensely stained for TMEM16A, whereas expression in larger primary arterioles or veins was weak or absent (Figure 4, B and C). Notably, the TMEM16A signal appeared to be particularly intense in cells located at vascular branching points (Figure 4C, arrows). To examine whether our immunohistochemical results corresponded with the distribution of functional TMEM16A channels, we performed patch-clamp recordings on tissue prints of retinal microvascular complexes. While no CaCCs were found in VSMCs of primary arterioles in the retina (Figure 4, D and G), tail current densities recorded from dome-shaped intermediate cells or pericytes of secondary and higher-order arterioles of wild-type retina were more than 3 times larger than those in the aorta (Figure 4, E and G). Similar currents were recorded from pericytes from microvascular complexes isolated from WT brain and were absent in cells of the conditional knockout (Figure 4, F and G, and Supplemental Figure 3, A and B).

The special 2-dimensional structure of the retina also allowed us to quantify vasoconstriction of second-order retinal arterioles in response to U46619 using time-lapse microscopy. While no difference between vessels from control and conditional knockout mice was found for saturating drug concentrations, constriction was reduced at submaximal levels in preparations from conditional knockout mice (Figure 4H and Supplemental Figure 3C), indicating a regulatory role for TMEM16A in retina microcirculation.

TMEM16A plays a more general role in small arterioles. Because of the hypotensive effect of the VSMC-specific TMEM16A disruption, we hypothesized that TMEM16A might play a more general role in small arterioles/capillaries. Indeed, in analogy to our findings in brain and retina, we also detected TMEM16A in small arterioles and capillaries of skeletal muscle (Figure 5A), while expression in larger arterial vessels was weak or absent. CaCCs were large in skeletal muscle pericytes of WT mice and absent in pericytes isolated from skeletal muscle of TMEM16A mutant mice (Figure 5, B and C).

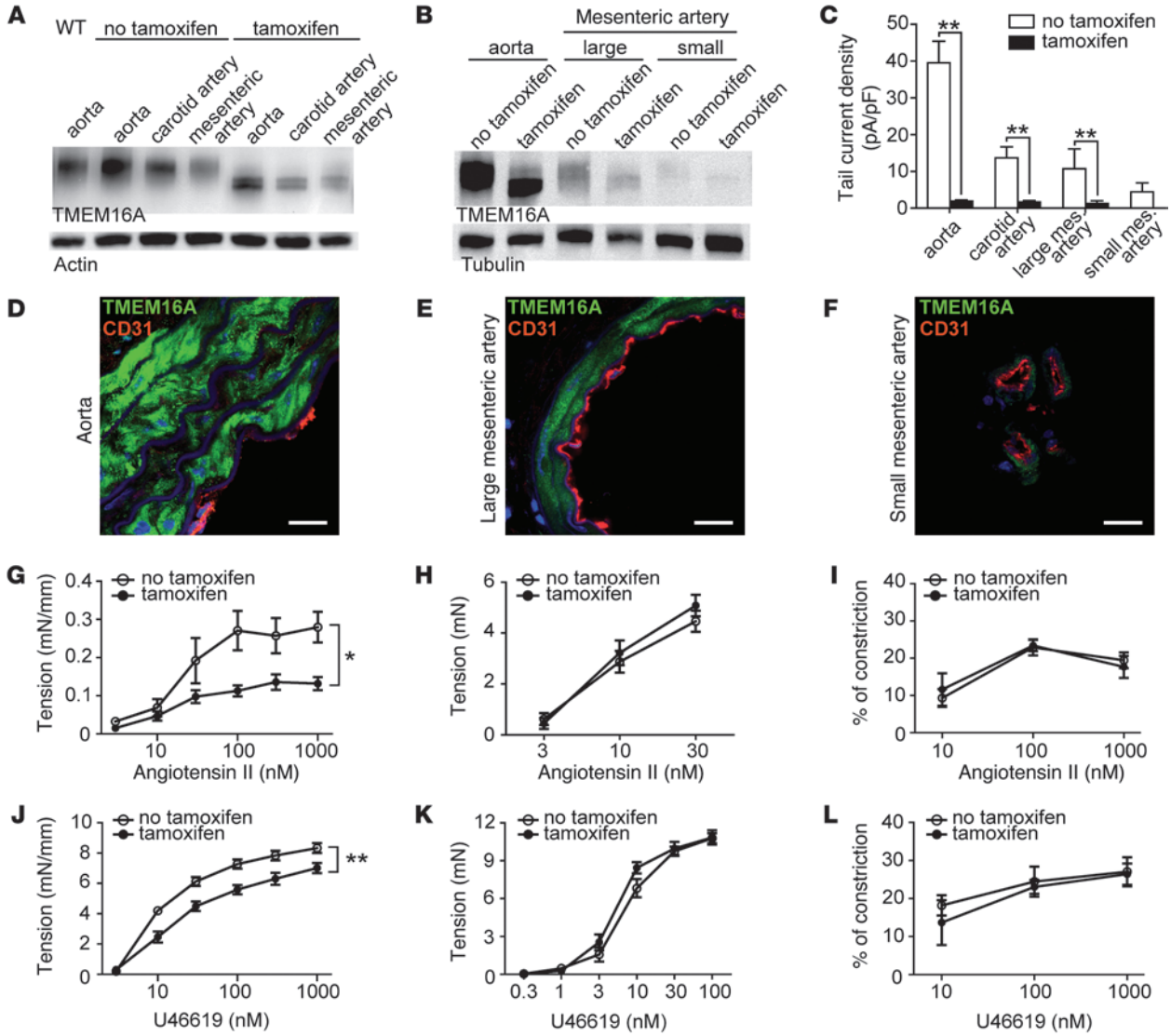

Figure 3

TMEM16A is expressed in the aorta and modulates its contractility but absent from medium-sized arteries. (**A** and **B**) Western blot analysis of protein lysates of isolated arterial blood vessels of non-induced control mice revealed that TMEM16A expression is particularly strong in the aorta as compared with carotid and mesenteric arteries. In tamoxifen-induced conditional *Tmem16a* knockout mice, the bands corresponding to TMEM16A were shifted to a smaller size. (**C**) Tail currents as a measure for the size of CaCCs in VSMCs isolated from different blood vessels differed significantly in size. In the induced conditional knockout, currents were abolished (n = 10–15 in each group). mes., mesenteric. (**D**–**F**) Whereas vascular smooth muscle cells in cryosections of the aorta of control mice were robustly stained (**D**), staining was less intense in large (**E**) and almost absent in small mesenteric arteries (**F**). Endothelial cells were stained with an antibody recognizing CD31. Scale bars: 30 μm. (**G**, **H**, **J**, and **K**) Dose-response curves for the contractile effects of angiotensin II (**G** and **H**) and U46619 (**J** and **K**) for aortic (**G** and **J**; n = 6 in each group) and first/second-order mesenteric artery rings (**H** and **K**; n = 16–24 in each group), as determined by wire myography. (**I** and **L**) Changes in diameter of pressurized third/fourth-order mesenteric arteries in response to different concentrations of angiotensin II (**I**) and U46619 (**L**), as determined by videomicroscopy (n = 4–6 in each group). Arteries of the two genotypes showed comparable dilator responses of roughly 25% to Ca^{2+}-free solutions (data not shown). 2-way ANOVA; *P < 0.05; **P < 0.01.

The influence of TMEM16A on the resting membrane potential and U46619-induced depolarization of skeletal muscle pericytes was determined using gramicidin-perforated patch recordings. While no significant difference between the genotypes was found for the resting membrane potential (Figure 5D), U46619-induced depolarization of WT pericytes was almost absent in the mutant (Figure 5E). In some cells U46619 caused fluctuations of the membrane potential, which may be explained by Ca^{2+} oscillations (31). These cells were excluded from the analysis. Other TMEM16A-deficient pericytes hyperpolarized after agonist application, which suggests the presence of Ca^{2+}-activated K^+ channels. Replacing Cl^- with methanesulfonate further increased the depolarization in WT, but not in mutant, pericytes (Figure 5E), indicating that Cl^- ion flow is important for U46619-induced pericyte depolarization.

To address whether CaCCs are relevant for the contractility of not only arterioles in the CNS but also peripheral blood vessels, we

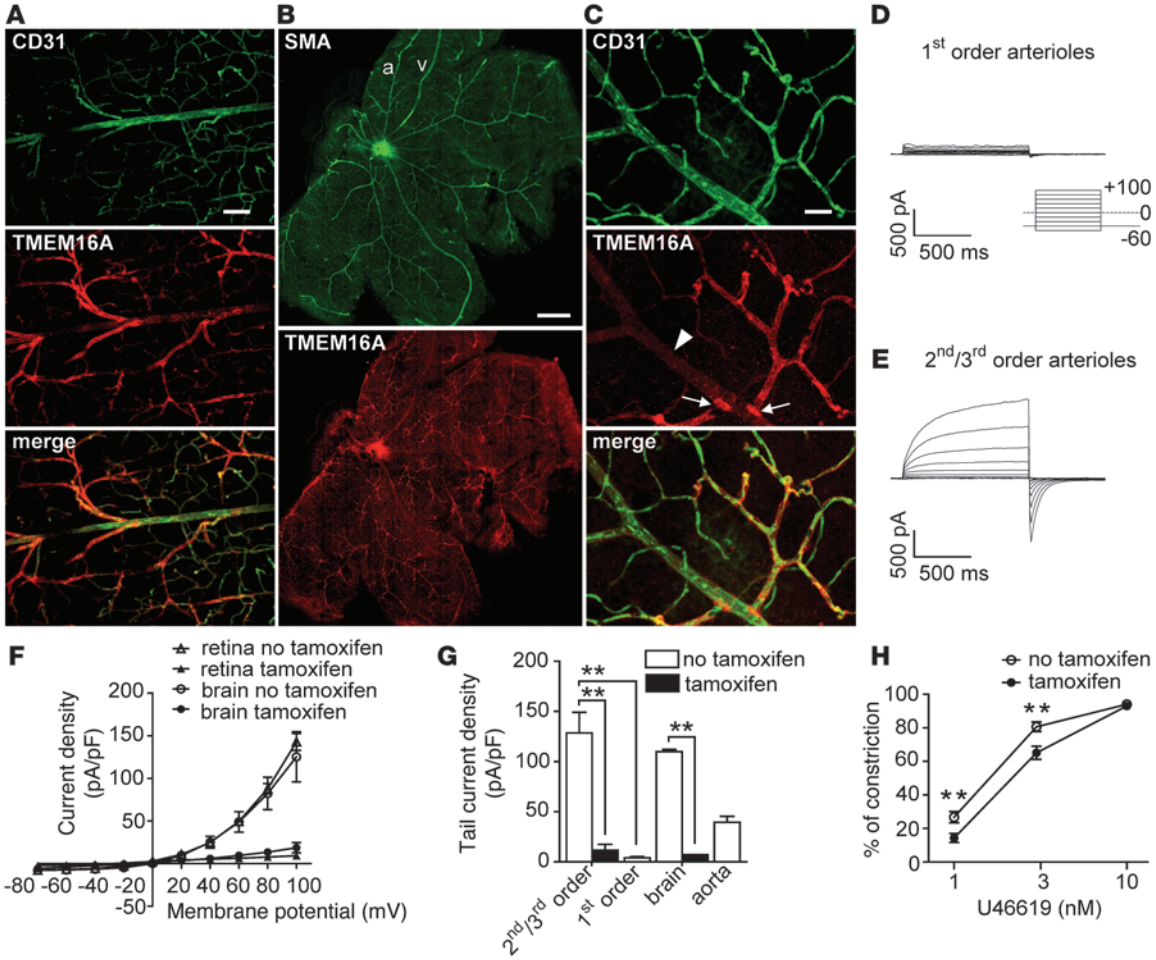

Figure 4

TMEM16A is expressed in small arterioles of brain and retina and enhances contractility in the retina. (**A**) Immunostaining of brain slices for the endothelial cell marker CD31 (upper) and TMEM16A (middle); the bottom panel shows an overlay. Small but not large arterioles show strong TMEM16A staining. Scale bar: 50 μm. (**B**) Epifluorescence images of retinal whole mount preparation stained for smooth muscle actin (SMA, upper) and TMEM16A (lower). Primary arterioles (a) and primary veins (v) originate from the optical disc in an alternate manner. Whereas TMEM16A staining in primary arterioles was absent or week, secondary and higher-order arterioles were intensely labeled. Scale bar: 300 μm. (**C**) Retina whole mount immunostainings for CD31 (upper) and TMEM16A (middle) showing a TMEM16A-negative primary arteriole (arrowhead) and second- and higher order arteriolar branches and overlay (lower). Arrows indicate strongly labeled cells at branching points of second-order arterioles. Scale bar: 30 μm. (**D**) Typical wild-type currents recorded from retina tissue prints of VSMC-like cells of first-order arterioles and (**E**) dome-shaped cells primarily found on second/third-order arterioles. The voltage protocol for **D** and **E** is shown in **D**. (**F**) CaCCs were absent in contractile cells of conditional knockout mice. (**G**) Mean tail current densities of contractile cells of the retina and brain arterioles for different genotypes and comparison with currents from VSMCs of the aorta (n = 6–17 each). (**H**) Constriction of second/third-order arterioles was diminished in the absence of CaCCs. Dose-response curves for U46619 in non-induced control and conditional *Tmem16a* knockout mice (n = 60 each). Student's t test; $^{**}P < 0.01$.

perfused isolated legs of WT and mutant mice at a constant flow rate and recorded the perfusion pressure. Although the perfusion pressure did not differ between genotypes under steady-state conditions, the pressure response to a bolus injection of U46619 (Figure 5F) was attenuated in TMEM16A mutant mice (Figure 5G). This finding strongly supports a role of TMEM16A in the contractility of peripheral microvessels, e.g., in skeletal muscle or skin.

Discussion

CaCCs were substantial in VSMCs of large conduit arteries, but small or absent in VSMCs of medium-sized arteries and large arterioles. In contrast, intermediate cells/pericytes of small arterioles displayed particularly strong CaCCs. As disruption of TMEM16A in contractile cells along the vascular tree lowered systemic blood pressure, eliminated vascular CaCCs, and diminished GPCR vasoconstrictor responses, we propose that TMEM16A is an important determinant of peripheral vascular resistance and thereby contributes to systemic blood pressure.

Supporting that CaCCs are relevant in the aorta, aortic ring preparations from knockout mice were less contractile in response to various agonists. The relative difference was more prominent in response to angiotensin II and phenylephrine when compared with U46619. This might reflect differences in the excitation-contraction coupling. Apart from Ca^{2+}-dependent pathways,

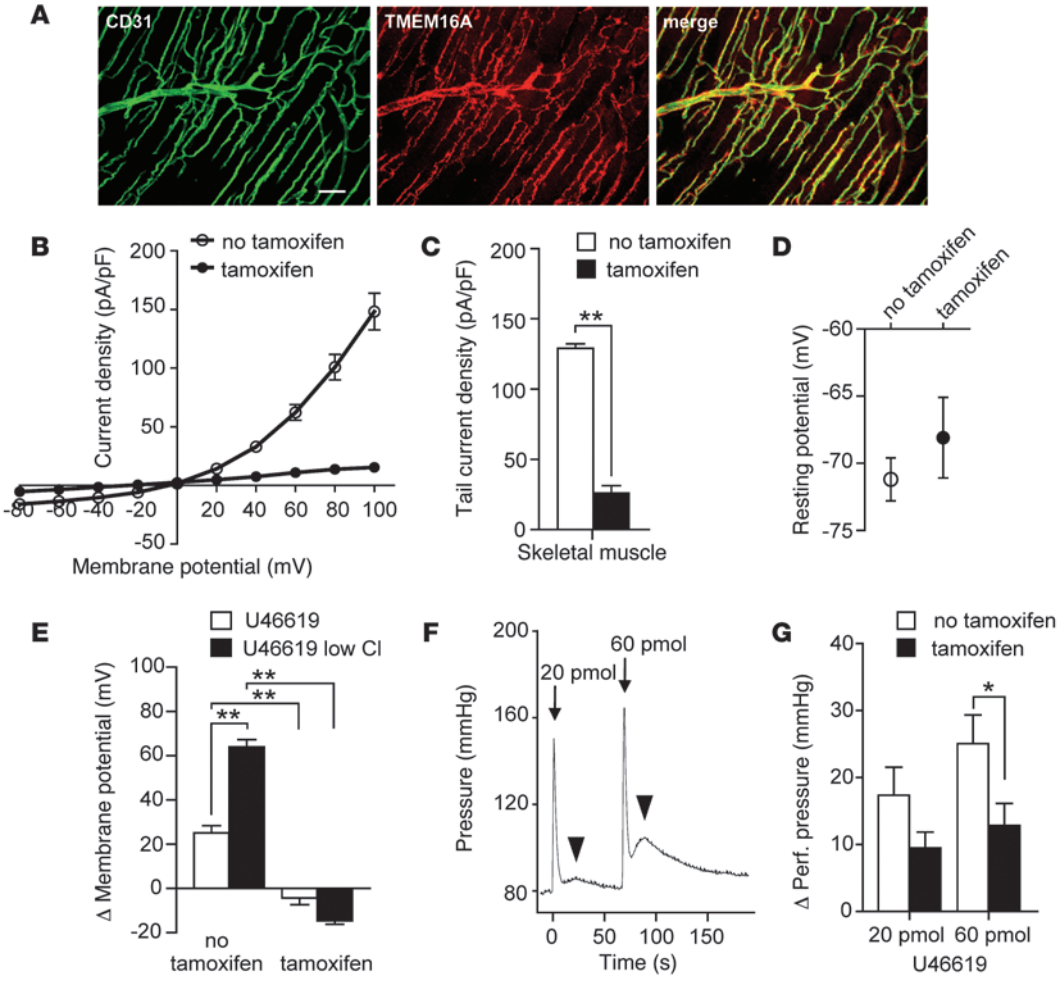

Figure 5

TMEM16A modulates peripheral resistance. (**A**) Double immunostaining for CD31 (left) and TMEM16A (center) of slices from skeletal muscle. The overlay is shown on the right. Scale bar: 50 μm. (**B** and **C**) I-V relationship (**B**) and tail current density (**C**) from isolated pericytes from skeletal muscle showed a drastic reduction of CaCCs upon disruption of TMEM16A (n = 13–16 cells each). $^{**}P < 0.01$. (**D**) Resting membrane potentials of isolated skeletal muscle pericytes did not differ between genotypes. $n = 6$; Student's t test; $P > 0.05$. (**E**) U46619-induced depolarization of WT pericytes was almost absent in the mutant. TMEM16A-deficient pericytes hyperpolarized after agonist application, which suggests the presence of Ca^{2+}-activated K^+ channels. Replacing Cl^- with methanesulfonate further increased the depolarization in WT, but not in mutant pericytes, indicating that Cl^- ion flow is important for U46619-induced pericyte depolarization. $n = 6$; Student's t test; $^{**}P < 0.01$. (**F**) Original tracing of the perfusion pressure of an isolated hind limb perfusion of a control mouse. The bolus injection of either 20 pmol or 60 pmol U46619 (arrows) caused a short pressure peak because of the injected volume and subsequently a protracted pressure increase. The peak responses are indicated by arrowheads. (**G**) The difference between peak and steady-state pressure at the two doses of U46619 analyzed. perf., perfusion. $n = 20$. Student's t test; $^{*}P < 0.05$.

U46619-mediated vasoconstriction also depends on the activation of Rho/Rho kinase signaling via G proteins $G\alpha_{12}$-$G\alpha_{13}$ (32), whereas phenylephrine and angiotensin II mainly act on $G\alpha_q$-$G\alpha_{11}$, which activate Ca^{2+}/myosin light chain kinase–mediated signaling (24). Large-diameter blood vessels such as the aorta do not contribute significantly to systemic blood pressure. Their walls extend when the blood pressure rises during systole and recoil during diastole. The aorta thereby dampens the fluctuations in arterial blood pressure during the cardiac cycle (Windkessel effect; ref. 33). The relevance of CaCCs for the Windkessel effect is supported by the reduction of the pulse pressure in our mutant mice.

CaCCs in VSMCs of large- and medium-sized arteries were small or even absent, and the contractile responses of these blood vessels did not differ between genotypes. How can these data be reconciled with our observation that disruption of TMEM16A results in a decrease in systemic blood pressure? Whereas large- and medium-sized arteries only marginally contribute to peripheral resistance, peripheral resistance is mainly determined by small arterioles with diameters of 50 μm or even less (34). Importantly, CaCCs mediated by TMEM16A were particularly large in intermediate cells and pericytes of small brain and retinal arterioles compared with VSMCs of the aorta. In accordance with our electrophysiological data and compatible with a prominent role of CaCCs in the microcirculation, the contraction of second- and third-order arterioles of the retina was diminished in response to submaximal concentrations of U46619 in VSMC-specific *Tmem16a* knockout mice.

We asked whether TMEM16A might have a similar function in arterioles of other tissues such as skeletal muscle, which recruit approximately 20% of cardiac output during rest and up to 80% during exercise and thus significantly contribute to overall vascular resistance. As in brain and retina, small CaCCs in intermediate cells/pericytes of skeletal muscle arterioles were large in WT mice and absent upon disruption of TMEM16A. In isolated hind limb perfusions, where peripheral resistance is largely determined by the skeletal muscle and/or skin microvasculature, the vasopressor response to U46619 was attenuated upon disruption of TMEM16A. These findings fully support our assumption that TMEM16A plays a role in peripheral resistance and might explain the decrease in arterial blood pressure upon disruption of TMEM16A even in the absence of strong effects on the mesenteric circulation.

Our findings strengthen the emerging hypothesis that vascular contractility contributes to the long-term control of systemic blood pressure (35), which is also supported by some clinical studies (36). Evidence also comes from a recent mouse model with a VSMC-specific disruption of the mineralocorticoid receptor (37). Similar to our findings, these mice developed a reduced systemic blood pressure over time and showed a reduction in the vasopressor response to angiotensin II, without any defects in renal sodium handling or changes in vascular structure. Moreover, vasoconstriction to angiotensin II or thromboxane A2 was diminished. Further supporting this concept, a pronounced decrease in systemic blood pressure was observed upon VSMC-specific disruption of microRNAs (38), while overexpression of a myosin phosphatase inhibitory protein (CPI-17) in VSMCs increased systemic blood pressure (39).

To what extent TMEM16A might play a role in the vasculature of other tissues and to what degree long-term compensation of reduced blood pressure might occur needs to be tested in the future. Currently, we cannot exclude that TMEM16A disruption may also affect pericyte-rich vasa recta. Descending vasa recta arise from juxtamedullary efferent arterioles with a mean diameter of around 10 μm and are characterized by a continuous endothelium surrounded by contractile pericytes. Descending vasa recta isolated from outer medullary bundles have been shown to contract to various agonists including angiotensin II (40), an effect that is known to be modulated by Cl^- (41, 42). Vascular disruption of TMEM16A may thus also have an effect on renal NaCl reabsorption and the regulation of the extracellular fluid compartment as another determinant of arterial blood pressure. Indeed, medullary blood flow was reported to be reduced in several models of experimental hypertension (43).

There are conflicting results regarding the possible role of CaCCs in renin-secreting cells, which are specialized VSMCs and where CaCCs have also been described (44). In renin-secreting cells, membrane depolarization by activation of chloride channels was associated with a reduction in renin release (45). However, niflumic acid, which is considered to preferentially inhibit CaCCs, increased renin secretion (46).

Our observation that the renin-angiotensin-aldosterone system was not activated in conditional *Tmem16a* knockout mice, may argue against a major role of the kidney in the hypotensive response upon disruption of vascular CaCCs.

Notably, TMEM16A labeling appeared to be particularly strong at branching points of small arterioles, which is consistent with previous reports that pericytes at precapillary branching points are equipped with a specialized contractile apparatus (47). This suggests the idea that TMEM16A might play a role for the recruitment of downstream capillaries and, hence, the channeling of nutrient supply. TMEM16A may also play important roles in pathological conditions such as pulmonary hypertension and stroke. Large CaCCs most likely mediated by TMEM16A have been reported for VSMCs of the pulmonary artery (18). Experimental occlusion of the middle cerebral artery induced a sustained contraction of downstream capillary pericytes, which remained contracted for hours despite reopening of the occluded vessel (48). This impaired microcirculatory reflow phenomenon negatively affects tissue survival and may in part depend on CaCCs, which are prominently expressed in pericytes, as shown in our study. This could be also relevant for other tissues such as the heart or renal medulla, which are known to be very vulnerable to ischemia.

Whether TMEM16A proves to be a target for therapy in humans in arterial hypertension or other pathological settings will be an important question to address in the future.

Methods

Mice

A genomic clone of murine *Tmem16a* including exon 21 was isolated from a 129/Sv mouse genomic library (λFixII; Stratagene) and was cloned into the pKO targeting vector. A diphtheria toxin A (DTA) cassette was introduced at the 3′ end of the targeting construct as a negative selection marker. A floxed neomycin selection cassette was cloned into the *Eco*RV restriction site 5′ of exon 21. A third loxP site was introduced into the *Afe*I restriction site 3′ of exon 21. This targeting vector was linearized via *Not*I and electroporated into R1 embryonic stem cells, which are derived from the SvJ line. Neomycin-resistant clones were screened for homologous recombination by Southern blot analysis of a genomic *Eco*RI digest with an external probe exploiting a novel *Eco*RI restriction site introduced with the third loxP site. Neomycin-resistant clones that had undergone homologous recombination were transfected with a plasmid expressing Cre recombinase (49). Resulting clones were tested for the extent of the DNA excision. A clone with a deletion of the neomycin selection cassette was injected into C57BL/6 blastocysts and transferred into foster mice. The floxed line was backcrossed with C57BL/6. Mice were genotyped by PCR using primers loxP-fwd (5′-CTCGGTGTGGGACTATGAACC-3′) and loxP-rev (5′-CAGATACACCCAGTGTTTCTCC-3′). The junction fragment upon deletion of exon 21 was amplified with the loxP-fwd primer and the primer KO-fwd (5′-CTCAGGCT CCCATGATCCTC-3′). Experiments were performed in F_5 on a mixed SvJ/C57BL/6 background.

The SMMHC-Cre-ER^{T2} (24) line was a gift from Stefan Offermanns, Max-Planck-Institut für Herz- und Lungenforschung, Bad Nauheim, Germany.

cDNA cloning. A TMEM16A-containing expressed sequence tag (IMAGE Consortium cDNA clone 30547439) was subcloned into the first multiple cloning site of the bicistronic pIRES vector (Clontech), containing GFP downstream of the IRES. cDNA corresponding to exon 21 was removed using standard PCR mutagenesis.

Antibodies

Polyclonal antibodies were raised in rabbits against the N-terminal mouse TMEM16A peptide RSVKQDHPLPGKGAS coupled to keyhole limpet hemocyanin. The resulting antisera were affinity purified. One purified antiserum detected TMEM16A in tissue protein lysates and tissue sections.

Western blotting

Tissues were ground in liquid nitrogen and homogenized in lysis buffer containing 50 mM Tris, 150 mM NaCl, 1 mM EDTA, 1% Triton X-100, 1 mM Na_3VO_4, 1 mM NaF, 2.5 mM Na_2HPO_4, 2.5 mM NaH_2O_4, 1 mM PMSF, and the Roche protease inhibitor cocktail. The samples were sonicated on

ice for 30 minutes and centrifuged at 3,100 *g* for 5 minutes to remove cell debris. The supernatant was collected, and the protein concentration was determined using the Pierce BCA Protein Assay Kit. 10 μg of protein was separated by 8% SDS-PAGE and transferred onto nitrocellulose membranes. The membranes were blocked with 3% blocking buffer (dry milk in TBS-T) and incubated with rabbit antibody against TMEM16A (1:500) in 1% blocking buffer or mouse anti–β-actin (1:2,000, Santa Cruz Biotechnology Inc.) or rabbit anti–α-tubulin (1:2,000, Abcam) in 3% blocking buffer overnight at 4°C. After the membranes were washed, they were incubated with HRP-conjugated anti-rabbit (1:2,000, Amersham Biosciences) or anti-mouse (1:2,000, Amersham Biosciences) secondary antibodies in 3% blocking buffer for 2 hours at room temperature (RT). Signals were detected with the ECL system (Millipore).

Cell culture and transfection

HEK293 cells were cultured under standard conditions (37°C, 5% CO_2) in DMEM supplemented with 10% fetal bovine serum and 1% penicillin/streptomycin. Cells were transfected with a plasmid encoding either the WT or the variant TMEM16A devoid of exon 21 and eGFP (pIRES-EGFP, Clontech) using the Lipofectamine 2000 reagent (Invitrogen).

Immunohistochemistry

Stainings on cryosections. Arteries were removed and postfixed with 4% paraformaldehyde in PBS overnight. After dehydration in 30% sucrose in PBS, the vessels were cut into 20-μm-thick cryosections. The slices were hydrated with PBS, blocked with 5% normal goat serum and 0.25% Triton X-100 in PBS, and incubated with our polyclonal TMEM16A antibody (1:250) and a monoclonal rat antibody against CD31 (1:1,000, BioLegend) in PBS overnight at 4°C. The slices were washed 3 times with PBS and incubated with Cy5-conjugated AffiniPure Goat anti-Rabbit IgG (1:1,000, Jackson ImmunoResearch Laboratories) and Alexa Fluor 555–labeled Goat Anti-Rat IgG (1:1,000, Molecular Probes, Life Technologies) in PBS for 2 hours at RT. After a washing step with PBS, the nuclei were stained with Hoechst-33258 (1:10,000, Molecular Probes, Life Technologies) in PBS, and the sections were washed 3 times with PBS. The slices were mounted with Fluoromount-G (SouthernBiotech) and analyzed with a Leica TCS SP5 confocal scanning fluorescence microscope.

Whole mount retina stainings. Eyes were removed post mortem and retinae isolated in Ringer solution (137 mM NaCl, 5 mM KCl, 1.8 mM $CaCl_2$, 1 mM $MgCl_2$, 10 mM D-glucose, 5 mM HEPES, pH 7.4). Radial incisions were made to flat-mount retinae on black filter paper (Millipore AABP02500), photoreceptor side down, and samples were fixed for 20 minutes in 4% paraformaldehyde in 0.1 PBS at RT. Retinae were washed 3 times in TN buffer (150 mM NaCl, Tris-HCl, pH 7.6) and blocked with 3% donkey serum and 1% BSA in TN buffer with 0.5% Triton X-100 and 0.02% NaN_3 overnight at RT. After incubation with our polyclonal rabbit antibody against TMEM16A (1:500) and a smooth muscle actin monoclonal antibody (1:500, Thermo Scientific) in blocking solution for 5 days at 4°C, retinae were washed for 1 hour in TN buffer and labeled with Cy5-conjugated AffiniPure Goat Anti-Rabbit IgG (Jackson ImmunoResearch Laboratories) and Alexa Fluor 488–labeled Donkey Anti-Mouse IgG (1:500, Molecular Probes, Life Technologies) in blocking solution for 3 hours at RT, washed in TN buffer, and mounted in ProLong Gold antifade reagent (Life Technologies). For retina overviews, multiple individual images were taken using a Zeiss Observer Z1 epifluorescence microscope equipped with a CoolSNAP HQ^2 camera (Photometrics) and stitched together using MetaMorph acquisition software (Universal Imaging).

Brain slices. The brain was carefully removed, rinsed in ice-cold TN buffer, and glued to the stage of a vibrating blade microtome (Leica VT1200S). 300-μm-thick sagittal sections were fixed in 4% paraformaldehyde in 0.1 PBS for 20–30 minutes at RT, washed 3 times in TN buffer (pH 7.6), and processed as described for the retina.

Skeletal muscle slices. The paw of the hind limb of a WT mouse was cut open, and the extensor digitorum longus muscle was removed, embedded in 2.5% SeaPlaque GTG low-melting-point agarose (Cambrex), glued to the stage of the vibrating blade microtome, and processed as described for the retina.

Histological analysis

Wall-to-lumen ratios were determined in H&E-stained transversal sections of paraffin-embedded thoracic aortae and large and small mesenteric arteries.

Radiotelemetric blood pressure measurement

Mice with a minimum body weight of 23 g were anesthetized by intraperitoneal application of ketamine/xylazine adapted to body weight. Telemetric transmitters (PhysioTel PA-C10, Data Sciences International) were implanted subcutaneously, with the sensing tip placed in the aorta via the left carotid artery. After 10 days of recovery from surgery interventions and/or recordings (Dataquest A.R.T. software for acquisition and analysis) were started. Angiotensin II (1.5 $ng*g^{-1}*min^{-1}$) was infused for 14 days by subcutaneously implanted osmotic minipumps (Alzet, model 1002).

For investigation of the effects of salt intake, mice were fed with modified special diets (Altromin C1036) containing 0.2 g Na^+/kg (low salt), 3 g Na^+/kg (control), or 30 g Na^+/kg (high salt).

Heart ultrasound analysis

Cardiac function and heart dimensions were assessed by transthoracic echocardiography using the Vevo 2100 System (VisualSonics) before and 2 weeks after termination of tamoxifen treatment. Echocardiography was performed during isoflurane anesthesia adapted to breathing frequency.

Blood analysis and renal function

For determination of plasma renin activity and plasma angiotensin II, aldosterone, and atrial natriuretic peptide (ANP) levels, mice were preconditioned to anesthesia for 9 days. One hour prior to the night period, mice were anesthetized with isoflurane, and blood was withdrawn by retro-orbital bleeding into EDTA-coated cups. Plasma was obtained by centrifugation.

For plasma renin activity, plasma taken right at the beginning of retro-orbital bleeding was diluted and incubated with substrate (plasma from bilaterally nephrectomized rats) for 90 minutes at either 4°C or 37°C. Angiotensin I formation was determined by RIA (Byk & DiaSorin Diagnostics), and specific formation (37°C values) was corrected by subtraction of unspecific interference (4°C values). Plasma aldosterone levels were determined by RIA (Siemens), plasma ANP levels by EIA (Phoenix Pharmaceuticals), and plasma angiotensin II levels by ELISA (ENZO Life Science) after extraction as described by the manufacturer.

Plasma electrolytes were measured in blood collected from the retro-orbital plexus of isoflurane-anesthetized mice using an electrolyte analyzer with ion-selective electrodes (Spotchem EL SE-1520, Arkray).

For renal function studies, mice were housed in metabolic cages (Tecniplast metabolic cage for single mouse, type 304) for 4 days. Urine was collected on day 4 for 24 hours, and blood was collected at the end of day 4. The diet contained 3 g Na^+/kg (ROD 16-R, LASvendi).

Myography of isolated vessels

Contraction of isolated aortae and mesenteric arteries was measured using a conventional small vessel wire myograph (DMT 610M, Danish Myo Technology). Briefly, thoracic aortae and mesenteric beds were removed, quickly transferred to cold (4°C) oxygenated (95% O_2, 5% CO_2) physiological salt solution (PSS), and dissected into 2 mm rings. Perivascular fat and connective tissues were removed. Each ring was dispensed

between two stainless steel wires (diameter, 0.0394 mm) in a 2 ml organ bath. The organ bath was filled with PSS. The composition of PSS was 119 mM NaCl, 4.7 mM KCl, 1.2 mM KH_2PO_4, 25 mM $NaHCO_3$, 1.6 mM $CaCl_2$, 1.2 mM Mg_2SO_4, and 11.1 mM D-glucose. The bath solution was continuously oxygenated with a gas mixture of 95% O_2 and 5% CO_2 and kept at 37 °C (pH 7.4). The aortic rings were placed under tension of 0.3 g. The mesenteric rings were placed under a tension equivalent to that generated at 0.9 times the diameter of the vessel at 100 mmHg. The software Chart5 (AD Instruments Ltd.) was used for data acquisition and display. After an equilibration period of 60 minutes and before the start of the experiment, the vessels were contracted with 60 mM KCl to assess viability. Subsequently, the vessels were contracted with phenylephrine, U46619, or angiotensin II at the concentrations indicated. For calibration and details, see ref. 50.

Videomicroscopy of mesenteric vessels

Mice were killed, and mesenteric beds were removed and transferred to cold (4°C) oxygenated (95% O_2, 5% CO_2) PSS. Mesenteric arteries were mounted onto glass cannulae on both sides, allowing application of hydrostatic pressure to the vessel. Perivascular fat and connective tissues were removed. For calibration and details, see ref. 50. Vessels were superfused continuously with Krebs-Henseleit solution (95% O_2, 5% CO_2; pH 7.4, 37°C) of the following composition: 119 mM NaCl, 4.7 mM KCl, 25 mM $NaHCO_3$, 1.2 mM KH_2PO_4, 1.6 mM $CaCl_2$, 1.2 mM $MgSO_4$, 0.03 mM EDTA, and 11.1 mM D-glucose. The vessels were pressurized stepwise to 20, 40, 60, 80, or 100 mmHg using a pressure servocontrol system (Living Systems Instrumentation). The inner diameter of the vessels was measured with a video microscope (Nikon Diaphot) connected to a personal computer for data acquisition and analysis (HaSoTec). The vessels were allowed to equilibrate for 45–60 minutes before the start of experiments. At 80 mmHg, the vessels were contracted with 60 mM KCl. Subsequently, the arteries were contracted with phenylephrine, U46619, or angiotensin II added to the bath solution. The myogenic tone was assessed by application of external Ca^{2+}-free PSS.

Contraction measurements of retinal arterioles

Enucleated eyes were placed in Ca^{2+}-free solution containing 135 mM NaCl, 5 mM NaOH, 3 mM KCl, 2 mM $CaCl_2$, 1 mM $MgCl_2$, 10 mM HEPES, 10 mM glucose, 1 μM nifedipine; pH 7.4, adjusted to 300 mOsm with sucrose. Corneae and lenses were removed and the retinae separated from the pigment epithelium. Each retina was cut into 3–4 pieces and transferred to a solution comprising 135 mM NaCl, 5 mM NaOH, 3 mM KCl, 2 mM $CaCl_2$, 1.8 mM $MgSO_4$, 1 mM NaH_2PO_4, 10 mM HEPES, 10 mM D-glucose; osmolarity was adjusted with sucrose to 300 mOsm at pH 7.4. Retina pieces were kept at room temperature under a constant supply of carbogen. After equilibration for at least 2 hours, pieces were transferred into a petri dish with the bottom of the coverslip glass mounted at the microscope stage. DIC images were taken with a Zeiss Observer Z1 microscope and the ×63 glycerol immersion objective using MetaMorph acquisition software. From each piece, several areas with blood vessels were selected for time-lapse imaging. Typically 7–10 areas of secondary and tertiary arterioles were collected every 30 seconds. Every 20 minutes U46619 was applied to achieve a final concentration of 1, 3, or 10 nM. For the analysis, the site of maximal constriction along the vessel was chosen and the diameter measured just before (control) or 20 minutes after administration of U46619 with the respective concentration.

Smooth muscle cell isolation

Isolated aorta, carotid, or large mesenteric arteries were placed into ice-cold preparation solution (70 mM NaCl, 1 mM KCl, 2 mM $MgCl_2$, 10 mM glucose, 100 mM saccharose, 0.5 mg/l BSA, 8% GlutaMAX [Life Technologies], 10 mM HEPES; pH 7.4), cut longitudinally, rinsed several times to remove blood, and cleaned of fat tissue. Afterward, samples were transferred into a microcentrifuge tube containing 250 μl digestion solution (preparation solution with 0.25 mg/ml elastase (Sigma-Aldrich) and 0.7 mg/ml collagenase type I (Sigma-Aldrich) and shaken at 350 rpm for 20 minutes at 37°C. After an additional incubation in fresh digestion solution for a further 20 minutes, tissue pieces were transferred into preparation solution and triturated using a Pasteur pipette. Dispensed cells were stored on ice until use for up to 3 hours.

Microvessel preparation for pericyte recordings

Retina microvessels were obtained using the tissue print method (51) with minor modifications. In brief, retina preparation solution contained 70 mM NaCl, 1 mM KCl, 2 mM $MgCl_2$, 10 mM glucose, 100 mM saccharose, 0.5 mg/l BSA, 8% GlutaMAX, 10 mM HEPES; pH 7.4, 310 mOsm. Instead of mannitol, the osmolarity was adjusted with sucrose. Each retina was placed in 2 ml of the oxygenated digestion solution containing 250 U/ml of DNase I (Worthington) and 3–4 U/ml of papain (Worthington), incubated for 30 minutes at 30°C, and sandwiched between two glass coverslips. After separation, some microvessels adhered to the coverslip in contact with the vitreal side of the retina. Sandwiching usually was repeated 5–8 times to obtain multiple samples.

For brain microvessels, mouse brains were dissected and transferred into ice-cold brain preparation solution (retina preparation solution with $MgSO_4$ instead of $MgCl_2$). Samples were subsequently transferred into brain preparation solution supplemented with 1% collagenase NB4 (Serva) and 1% collagenase type II (Worthington) (digestion solution). After incubation at 37°C for 1 hour, samples were slowly triturated 3–4 times using a pipette tip with an opening of approximately 1 mm. After sedimentation digestion solution was carefully removed and replaced by brain preparation solution. The tissue suspension contained several microvessels and was kept at room temperature.

Skeletal muscle microvessels were isolated from triceps muscles. After dissection, muscles were placed into PSS containing 120 mM NaCl, 5 mM KCl, 1.2 mM $MgCl_2$, 1.6 mM $CaCl_2$, 1.2 mM NaH_2PO_4, 20 mM $NaHCO_3$, 10 mM glucose, pH 7.4, cleaned from fascia and debris, and slightly torn apart to improve access of enzymes. For digestion, each muscle was transferred into a 50 ml Falcon tube containing 10 ml PSS supplemented with 2.4% collagenase type II (Worthington), 16 mM GlutaMAX, and 100 U/ml Penicillin-Streptomycin and incubated for 50 minutes in a shaking incubator at 37°C and 170 rpm. Then 20 ml PSS was added.

Perfused hind limb vasculature

Isolated hind limb perfusion was performed as described previously for isolated mesenteric vascular bed preparations (52), with some modifications (53, 54). In brief, dissected hind legs of briefly perfused mice (PSS: 137 mM NaCl, 5.4 mM KCl, 1.8 mM $CaCl_2$, 1 mM $MgCl_2$, 10 mM glucose, 10 mM HEPES, pH 7.4) were placed on a heated (37°C) plate and kept moist. Femoral arteries were cannulated and perfused using a peristaltic pump at a constant flow with gassed (95% O_2, 5% CO_2) PSS. Perfusion pressure was continuously determined by a pressure transducer (Living Systems Instrumentation) and recorded on a polygraph. After an equilibration period of 10 minutes, the flow rate was gradually increased until a perfusion pressure of 80 mmHg was reached to induce a spontaneous myogenic tone (54). When the pressure had stabilized, a bolus of U46616 was injected (either 20 or 60 pmol in a total volume of 200 μl) and the changes in perfusion pressure recorded. Since flow was maintained at a constant rate, changes in peripheral vascular resistance resulted in changes in perfusion pressure.

Electrophysiology

Currents from HEK cells or VSMCs/intermediate cells/pericytes were recorded in the whole-cell voltage-clamp mode, using an EPC-10 amplifier and PatchMaster software (HEKA). The extracellular solution contained 140 mM NaCl, 5 mM KCl, 2 mM $MgCl_2$, 1.4 mM $CaCl_2$, 20 mM TEA, 10 mM D-glucose, 10 mM HEPES; adjusted to pH 7.4. Patch pipettes were pulled from borosilicate glass capillaries (1.5 mm O.D., 1.2 mm I.D.); pipette resistance was typically 3–4 MOhm. Patch pipettes were filled with a solution containing 140 mM CsCl, 1.2 mM $MgCl_2$, 1.4 mM $CaCl_2$, 10 mM HEDTA, 20 mM TEA, 10 mM HEPES; adjusted to pH 7.2 with CsOH. Free $[Ca^{2+}]_i$ was 600 nM, determined using a NanoDrop 3300 fluorescence spectrometer (Thermo Fisher) and the ratiometric indicator Indo1 (Invitrogen). In some experiments, a calcium-free intracellular solution was used devoid of $CaCl_2$ and supplemented with 10 mM EGTA. The osmolarity of all extra- and intracellular solutions was approximately 310 mOsm. Recordings were made at RT. The holding potential was –60 mV. To determine the voltage dependence of activation, a series of depolarization steps (1 second duration) from –80 to +100 mV was applied with 20 mV increments. Steady-state current amplitudes were measured at the end of the depolarization pulse. Tail currents were more appropriate for quantification because prolonged depolarization activated an unrelated outward rectifying conductance in some cells but had no effect on tail currents. The amplitude of tail currents was determined at –80 mV after depolarization to +80 mV by fitting the tail current trace with a mono-exponential function using FitMaster software (HEKA). For patch-clamp recordings from retina pericytes, the extracellular solution contained 135 mM NaCl, 5 mM NaOH, 3 mM KCl, 2 mM $CaCl_2$, 1 mM $MgCl_2$, and 10 mM HEPES; 300 mOsm, pH 7.4.

For recordings of brain and skeletal muscle pericytes, 0.5 ml of the tissue suspension was mixed with either 2.5 ml of brain preparation solution or PSS and placed in a glass petri dish. Microvessels were allowed to settle. Exchange of solutions was performed by a pressure-driven perfusion system (ALA-VM8; ALA Scientific Instruments).

In perforated patch-clamp recordings, pipette solution contained 130 mM KCl, 10 mM NaCl, 3 mM $CaCl_2$, 1.2 mM $MgCl_2$, 10 mM HEDTA, 10 mM HEPES, adjusted to pH 7.2 with KOH. Gramicidin (G5002, Sigma-Aldrich) was added at a final concentration of 5 μg/ml from a stock solution.

Statistics

Data are shown as mean ± SEM, and *n* represents the number of animals, specimen, or cells. Statistical analysis was performed by 2-tailed unpaired Student's *t* test or 2-way ANOVA, if not stated otherwise. Mean arterial blood pressure was also compared by the Bonferroni post hoc analysis. A *P* value less than 0.05 was considered statistically significant.

Study approval

Animal experiments were performed according to and with approval of Thüringer Landesamt für Verbraucherschutz, Bad Langensalza; Germany, Landesamt für Gesundheit und Soziales, Berlin, Germany; and Amt für Verbraucherschutz, Lebensmittelsicherheit und Veterinärwesen, Hamburg, Germany.

Acknowledgments

We thank Stefan Offermanns for the opportunity to use the SMMHC-Cre-ER^{T2} line. We thank Karin Dedek for suggestions and comments on retina experiments. We further acknowledge excellent technical support by Katrin Schorr and Yoland-Marie Anistan. Christian A. Hübner is funded by the Deutsche Forschungsgemeinschaft (DFG), the Bundesministerium für Bildung und Forschung (BMBF), the Interdisziplinäres Zentrum für Klinische Forschung (IZKF) Jena, and the Thyssen Foundation. Björn C. Schroeder received funding from the Thyssen Foundation and NeuroCure. Heimo Ehmke is funded by the Deutsches Zentrum fur Herz-Kreislauf-Forschung (DZHK). Maik Gollasch is funded by the DFG. Maik Gollasch is funded by the DFG.

Received for publication March 20, 2013, and accepted in revised form October 24, 2013.

Address correspondence to: Christian A. Hübner, Institut für Humangenetik, Universitätsklinikum Jena, Kollegiengasse 10, 07743 Jena, Germany. Phone: 0049.3641.935500; Fax: 0049.3641.935502; E-mail: christian.huebner@med.uni-jena.de. Or to: Björn C. Schroeder, Max-Delbrück Centrum für Molekulare Medizin (MDC), Robert-Rössle-Straße 10, 13125, Berlin, Germany. Phone: 0049.30.94062264; Fax: 0049.30.94063327; E-mail: bjoern.schroeder@mdc-berlin.de.

1. Kearney PM, Whelton M, Reynolds K, Muntner P, Whelton PK, He J. Global burden of hypertension: analysis of worldwide data. *Lancet*. 2005; 365(9455):217–223.
2. Cowley AW Jr. A tribute to Eric Muirhead. Evolution of the Medullipin concept of blood pressure control. *Nephrol Dial Transplant*. 1995;10(7):1137–1141.
3. Orlov SN, Tremblay J, Hamet P. NKCC1 and hypertension: a novel therapeutic target involved in the regulation of vascular tone and renal function. *Curr Opin Nephrol Hypertens*. 2010;19(2):163–168.
4. Matchkov VV, Aalkjaer C, Nilsson H. Distribution of cGMP-dependent and cGMP-independent Ca2+-activated Cl- conductances in smooth muscle cells from different vascular beds and colon. *Pflugers Arch*. 2005;451(2):371–379.
5. Rust MB, et al. Neurogenic mechanisms contribute to hypertension in mice with disruption of the K-Cl cotransporter KCC3. *Circ Res*. 2006; 98(4):549–556.
6. Byrne NG, Large WA. Membrane ionic mechanisms activated by noradrenaline in cells isolated from the rabbit portal vein. *J Physiol*. 1988;404:557–573.
7. Large WA, Wang Q. Characteristics and physiological role of the Ca2+-activated Cl- conductance in smooth muscle. *Am J Physiol*. 1996;271(2 pt 1):C435–C454.
8. Leblanc N, et al. Regulation of calcium-activated chloride channels in smooth muscle cells: a complex picture is emerging. *Can J Physiol Pharmacol*. 2005;83(7):541–556.
9. Caputo A, et al. TMEM16A, a membrane protein associated with calcium-dependent chloride channel activity. *Science*. 2008;322(5901):590–594.
10. Schroeder BC, Cheng T, Jan YN, Jan LY. Expression cloning of TMEM16A as a calcium-activated chloride channel subunit. *Cell*. 2008;134(6):1019–1029.
11. Yang YD, et al. TMEM16A confers receptor-activated calcium-dependent chloride conductance. *Nature*. 2008;455(7217):1210–1215.
12. Charlesworth G, et al. Mutations in ANO3 cause dominant craniocervical dystonia: ion channel implicated in pathogenesis. *Am J Hum Genet*. 2012; 91(6):1041–1050.
13. Bolduc V, et al. Recessive mutations in the putative calcium-activated chloride channel Anoctamin 5 cause proximal LGMD2L and distal MMD3 muscular dystrophies. *Am J Hum Genet*. 2010;86(2):213–221.
14. Suzuki J, Umeda M, Sims PJ, Nagata S. Calcium-dependent phospholipid scrambling by TMEM16F. *Nature*. 2010;468(7325):834–838.
15. Vermeer S, et al. Targeted next-generation sequencing of a 12.5 Mb homozygous region reveals ANO10 mutations in patients with autosomal-recessive cerebellar ataxia. *Am J Hum Genet*. 2010;87(6):813–819.
16. Malvezzi M, et al. Ca2+-dependent phospholipid scrambling by a reconstituted TMEM16 ion channel. *Nat Commun*. 2013;4:2367.
17. Davis AJ, et al. Expression profile and protein translation of TMEM16A in murine smooth muscle. *Am J Physiol Cell Physiol*. 2010;299(5):C948–C959.
18. Manoury B, Tamuleviciute A, Tammaro P. TMEM16A/anoctamin 1 protein mediates calcium-activated chloride currents in pulmonary arterial smooth muscle cells. *J Physiol*. 2010;588(pt 13):2305–2314.
19. Bulley S, et al. TMEM16A/ANO1 channels contribute to the myogenic response in cerebral arteries. *Circ Res*. 2012;111(8):1027–1036.
20. Thomas-Gatewood C, et al. TMEM16A channels generate Ca2+-activated Cl- currents in cerebral artery smooth muscle cells. *Am J Physiol Heart Circ Physiol*. 2011;301(5):H1819–H1827.
21. Wang M, et al. Downregulation of TMEM16A calcium-activated chloride channel contributes to cerebrovascular remodeling during hypertension by promoting basilar smooth muscle cell proliferation. *Circulation*. 2012;125(5):697–707.
22. Rock JR, Futtner CR, Harfe BD. The transmembrane protein TMEM16A is required for normal development of the murine trachea. *Dev Biol*. 2008;321(1):141–149.
23. Schwenk F, Baron U, Rajewsky K. A cre-transgenic mouse strain for the ubiquitous deletion of loxP-flanked gene segments including deletion in germ cells. *Nucleic Acids Res*. 1995;23(24):5080–5081.
24. Wirth A, et al. G12-G13-LARG-mediated signaling in vascular smooth muscle is required for salt-induced hypertension. *Nat Med*. 2008;

14(1):64–68.
25. Kiermayer C, Conrad M, Schneider M, Schmidt J, Brielmeier M. Optimization of spatiotemporal gene inactivation in mouse heart by oral application of tamoxifen citrate. *Genesis*. 2007;45(1):11–16.
26. Levick RJ. *An Introduction Into Cardiovascular Physiology*. 5th ed. Boca Raton, Florida, USA: CRC Press; 2011.
27. Sims DE. The pericyte — a review. *Tissue Cell*. 1986; 18(2):153–174.
28. Dalkara T, Gursoy-Ozdemir Y, Yemisci M. Brain microvascular pericytes in health and disease. *Acta Neuropathol*. 2011;122(1):1–9.
29. Sakagami K, Wu DM, Puro DG. Physiology of rat retinal pericytes: modulation of ion channel activity by serum-derived molecules. *J Physiol*. 1999;521(part 3):637–650.
30. Armulik A, Genove G, Betsholtz C. Pericytes: developmental, physiological, and pathological perspectives, problems, and promises. *Dev Cell*. 2011;21(2):193–215.
31. Zhang Q, Cao C, Zhang Z, Wier WG, Edwards A, Pallone TL. Membrane current oscillations in descending vasa recta pericytes. *Am J Physiol Renal Physiol*. 2008;294(3):F656–F666.
32. Loirand G, Guerin P, Pacaud P. Rho kinases in cardiovascular physiology and pathophysiology. *Circ Res*. 2006;98(3):322–334.
33. Belz GG. Elastic properties and Windkessel function of the human aorta. *Cardiovasc Drugs Ther*. 1995;9(1):73–83.
34. Levy BI, Ambrosio G, Pries AR, Struijker-Boudier HA. Microcirculation in hypertension: a new target for treatment? *Circulation*. 2001;104(6):735–740.
35. Mendelsohn ME. In hypertension, the kidney is not always the heart of the matter. *J Clin Invest*. 2005;115(4):840–844.
36. Taylor RS, Ashton KE, Moxham T, Hooper L, Ebrahim S. Reduced dietary salt for the prevention of cardiovascular disease: a meta-analysis of randomized controlled trials (Cochrane review). *Am J Hypertens*. 2011;24(8):843–853.
37. McCurley A, et al. Direct regulation of blood pressure by smooth muscle cell mineralocorticoid receptors. *Nat Med*. 2012;18(9):1429–1433.
38. Albinsson S, et al. Smooth muscle miRNAs are critical for post-natal regulation of blood pressure and vascular function. *PLoS One*. 2011;6(4):e18869.
39. Su W, Xie Z, Liu S, Calderon LE, Guo Z, Gong MC. Smooth muscle-selective CPI-17 expression increases vascular smooth muscle contraction and blood pressure. *Am J Physiol Heart Circ Physiol*. 2013;305(1):H104–H113.
40. Pallone TL, Zhang Z, Rhinehart K. Physiology of the renal medullary microcirculation. *Am J Physiol Renal Physiol*. 2003;284(2):F253–F266.
41. Pallone TL, Huang JM. Control of descending vasa recta pericyte membrane potential by angiotensin II. *Am J Physiol Renal Physiol*. 2002;282(6):F1064–F1074.
42. Zhang Z, Huang JM, Turner MR, Rhinehart KL, Pallone TL. Role of chloride in constriction of descending vasa recta by angiotensin II. *Am J Physiol Regul Integr Comp Physiol*. 2001;280(6):R1878–R1886.
43. Cowley AW Jr, Roman RJ. The role of the kidney in hypertension. *JAMA*. 1996;275(20):1581–1589.
44. Kurtz A, Penner R. Angiotensin II induces oscillations of intracellular calcium and blocks anomalous inward rectifying potassium current in mouse renal juxtaglomerular cells. *Proc Natl Acad Sci U S A*. 1989;86(9):3423–3427.
45. Kurtz A. Renin release: sites, mechanisms, and control. *Annu Rev Physiol*. 2011;73:377–399.
46. Nabel C, Schweda F, Riegger GA, Kramer BK, Kurtz A. Chloride channel blockers attenuate the inhibition of renin secretion by angiotensin II. *Pflugers Arch*. 1999;438(5):694–699.
47. Bandopadhyay R, Orte C, Lawrenson JG, Reid AR, De Silva S, Allt G. Contractile proteins in pericytes at the blood-brain and blood-retinal barriers. *J Neurocytol*. 2001;30(1):35–44.
48. Yemisci M, Gursoy-Ozdemir Y, Vural A, Can A, Topalkara K, Dalkara T. Pericyte contraction induced by oxidative-nitrative stress impairs capillary reflow despite successful opening of an occluded cerebral artery. *Nat Med*. 2009;15(9):1031–1037.
49. Rust MB, et al. Disruption of erythroid K-Cl cotransporters alters erythrocyte volume and partially rescues erythrocyte dehydration in SAD mice. *J Clin Invest*. 2007;117(6):1708–1717.
50. Dietrich A, et al. Increased vascular smooth muscle contractility in TRPC6$^{-/-}$ mice. *Mol Cell Biol*. 2005;25(16):6980–6989.
51. Puro DG. Retinovascular physiology and pathophysiology: new experimental approach/new insights. *Prog Retin Eye Res*. 2012;31(3):258–270.
52. Fésüs G, et al. Adiponectin is a novel humoral vasodilator. *Cardiovasc Res*. 2007;75(4):719–727.
53. Mathar I, et al. Increased catecholamine secretion contributes to hypertension in TRPM4-deficient mice. *J Clin Invest*. 2010;120(9):3267–3279.
54. Moosmang S, et al. Dominant role of smooth muscle L-type calcium channel Cav1.2 for blood pressure regulation. *EMBO J*. 2003;22(22):6027–6034.